We are IntechOpen, the world's leading publisher of Open Access books Built by scientists, for scientists

4,800
Open access books available

122,000
International authors and editors

135M
Downloads

Our authors are among the

154
Countries delivered to

TOP 1%
most cited scientists

12.2%
Contributors from top 500 universities

CLARIVATE ANALYTICS BOOK CITATION INDEX INDEXED

WEB OF SCIENCE™

Selection of our books indexed in the Book Citation Index in Web of Science™ Core Collection (BKCI)

Interested in publishing with us?
Contact book.department@intechopen.com

Numbers displayed above are based on latest data collected.
For more information visit www.intechopen.com

13

Optimal Motion Planning for Manipulator Arms Using Nonlinear Programming

Jong-keun Park
Kyungnam University
South Korea

1. Introduction

The optimal motion planning problems for manipulator arms have been actively researched in robotics in the past two or three decades because the optimal motions that minimize actuator forces, energy consumption, or motion time yield high productivity, efficiency, smooth motion, durability of machine parts, etc. These merits are more apparent when the manipulator arms execute repeated motions.

This subject is roughly divided into two categories according to the tasks that the manipulator arms should perform. These categories are characterized by motions as with or without geometric path constraints.

If the geometric path of the end-effector of a non-redundant manipulator is predetermined, the motion has one degree of freedom (DOF) and can be represented by a scalar path variable. In this case, rigorous solutions were obtained subject to constant bounds on the actuator forces (Bobrow et al., 1985; Shin & McKay, 1985). Subsequently, the study was extended to cases where the path included certain singular points on it (Shiller, 1994) or where the actuator jerks and actuator torques were limited within constant bounds (Constantinescu & Croft, 2000).

Most manipulator tasks—except arc welding, painting or cutting—are essentially motions without geometric path constraints. In this case, obstacle avoidance should be considered simultaneously with motion optimization. These types of manipulator motions have the same DOF as the number of lower pair joints, and the corresponding optimal motions are more complicated than those discussed above. The subject of this chapter lies in this category.

Various types of methods have been developed to solve the optimal motion planning problem in the presence of obstacles. Optimal control theory (Bryson & Meier, 1990; Bessonnet & Lallemand, 1994; Formalsky, 1996; Galicki, 1998), nonlinear programming (Fenton et al., 1986; Bobrow, 1988; Singh & Leu, 1991), dynamic programming (Jouaneh et al., 1990), tessellation of joint (Ozaki & Lin, 1996) or configuration space (Shiller & Dubowsky, 1991), and a combination of these (Schlemmer & Gruebel, 1998; Hol et al., 2001) are the main techniques used.

By the application of the optimal control theory, Pontryagin's maximum principle leads to a two-point boundary value problem. Some researchers have attempted to solve these equations directly (Bryson & Meier, 1990; Formalsky, 1996) while others have attempted to

Source: Industrial Robotics: Programming, Simulation and Applicationl, ISBN 3-86611-286-6, pp. 702, ARS/plV, Germany, December 2006, Edited by: Low Kin Huat

solve them through parameter optimization (Hol et al., 2001). Although this theory and its solutions are rigorous, it has been used to solve equations for the motions of 2-link or at most 3-link planar manipulators due to the complexity and the nonlinearity of the manipulator dynamics.

Approximation methods have been studied to obtain the solutions for three or more DOF spatial manipulators; however, the solutions obtained have not been proved to be optimal. These approximation methods are roughly divided into two groups depending on whether or not they utilize gradients.

Most algorithms based on nonlinear programming use gradients (Fenton et al., 1986; Bobrow, 1988; Singh & Leu, 1991; Bobrow et al., 2001; Wang et al., 2001). For stable convergence, the objective functions and constraints must be locally convex and their first derivatives must be continuous. Numerically calculated gradients have been used to find minimum time motions (Bobrow, 1988); however, the simulation model was a 3-link spatial manipulator in the presence of a relatively simple obstacle model. Subsequently, analytically calculated gradients were used to minimize actuator torques for various multibody systems (Bobrow et al., 2001) or spatial 6-link manipulators (Wang et al., 2001). However, torque or energy minimizations show more stable convergence properties than the minimum time motions because the motion time is fixed.

Other approximation methods that do not utilize gradients are mainly based on (1) approximations in small time-intervals (Singh & Leu, 1991; Jouaneh et al., 1990; Hol et al., 2001) or (2) discretization/tessellation (Ozaki & Lin, 1996; Shiller & Dubowsky, 1991; Schlemmer & Gruebel, 1998) of joint or configuration spaces. The former requires less CPU time but may accumulate numerical or modeling errors in small time-intervals and thus lower the accuracy of the results. The latter assures stable convergence but the CPU time may increase exponentially for the refinement of tessellation.

Because of the complex dynamics and kinematics of robot manipulators, various assumptions or simplifications were introduced for the online implementation or simplification of the algorithms.

Using geometric simplifications, obstacles have been ignored (Bessonnet & Lallemand, 1994; Fenton et al., 1986; Jouaneh et al., 1990; Hol et al., 2001; Lee, 1995) or modeled as circles (Galicki, 1998; Singh & Leu, 1991; Ozaki & Lin, 1996) or as finite surface points (Schlemmer & Gruebel, 1998), and robot links have been modeled as lines (Galicki, 1998; Ozaki & Lin, 1996; Lee, 1995), finite surface points (Singh & Leu, 1991), or ellipsoids (Schlemmer & Gruebel, 1998).

Using kinematic simplifications, motions were restricted in a plane (Formalsky, 1996; Galicki, 1998; Ozaki & Lin, 1996; Shin & Zheng, 1992; Lee, 1995), the orientation of the end-effector was ignored (Singh & Leu, 1991; Shiller & Dubowsky, 1991), or the joint velocity profiles (Fenton et al., 1986) or joint acceleration profiles (Jouaneh et al., 1990; Schlemmer & Gruebel, 1998; Cao et al., 1998) were pre-specified.

Using dynamic simplifications, manipulator dynamics were ignored subject only to the kinematic constraints (Fenton et al., 1986; Shin & Zheng, 1992; Cao et al., 1998).

To the best of the author's knowledge, the optimal motions for six or more DOF manipulators or multiple robot arms have not yet been obtained without simplifying any of the geometric, kinematic, or dynamic models of manipulators or obstacles.

In this study, we transform the optimal control problem in a function space into a nonlinear programming problem in a finite-dimensional vector space. Joint displacements are

represented by the linear combinations of finite-term quintic *B*-splines. If a sufficient number of terms are used an exact solution will be obtained. Using numerically calculated gradients, the optimal coefficients of the splines are obtained.

The novel contribution made by this study is the concept of the *minimum overload trajectory* with fixed total motion time. The minimum time motions are defined rigorously by this concept and they are found successfully by the sequential searches for minimum overload trajectories. In the minimum overload searches, the convergence is quite stable because the performance index and all the constraints are locally convex and smooth and the total motion time is fixed.

To compute the minimum overload trajectory, the total motion time is initially specified to be very small so that the actuators require more force than they can produce. Then, using an efficient numerical optimization, the actuator overloads are minimized during the motion. Using the information obtained from the minimum overload trajectory, we predict the motion time of the next minimum overload search. These successive searches continue until we find the least time at which the minimum overload vanishes.

Obstacle information is evaluated by penetration growth distances (Ong & Gilbert, 1996), and obstacle avoidance is achieved by incorporating a penalty term that is included in an augmented performance index. The usefulness of the penetration growth distance will be shown in the simulation results.

The complete geometric, kinematic, and dynamic models of a spatial 6-link manipulator and the obstacles in its path are considered in this study. The effects of friction are the only variables that are ignored.

The manipulator dynamics are calculated by the outward and inward iteration method (Craig, 1986). This iteration method requires only joint-by-joint recursive calculations and accumulates a slight numerical error. In addition, it can be applied without knowing the equations of motions explicitly in higher DOF models.

In most of the other studies, the constraints on the actuator forces are constant, regardless of joint velocities. It is more practical for the bounds of the actuator forces to be dependent on the joint velocities, as was done in this study.

Trial applications to a spatial 3-link and a 6-link Puma 560 manipulator in the presence of polyhedral obstacles demonstrate the effectiveness and numerical stability of this algorithm.

2. Formulations of Optimal Motions

2.1 Actuator Characteristics

We consider two different actuator characteristics as shown in Fig. 1: One is that the actuator force limits depend on the joint velocities as shown in Fig. 1(a); the other is that the two limits are constant as shown in Fig. 1(b).

In most practical cases, the limits of the actuator forces are dependent on the joint velocities. In this case, the constraints on the actuators are as follows:

$$|\tau_i| \le -\frac{\tau_i^c}{\omega_i^c}|\omega_i| + \tau_i^c, \quad i = 1, \cdots, n \tag{1}$$

where τ_i and ω_i are the generalized actuator force and joint velocity of the i-th joint, respectively; τ_i^c, ω_i^c are the absolute values of their limits; n is DOF of the system, which is equal to the number of lower pair joints.

If we define *equivalent actuator forces* τ_i^e as

$$\tau_i^e = |\tau_i| + \frac{\tau_i^c}{\omega_i^c}|\omega_i|, \quad i = 1, \cdots, n \tag{2}$$

then the actuator constraints (1) become

$$\tau_i^e \le \tau_i^c, \quad i = 1, \cdots, n \tag{3}$$

If the limits are constant as shown in Fig. 1(b), the actuator and velocity constraints can be simply expressed as:

$$|\tau_i| \le \tau_i^c, \quad i = 1, \cdots, n \tag{4}$$

$$|\omega_i| \le \omega_i^c, \quad i = 1, \cdots, n \tag{5}$$

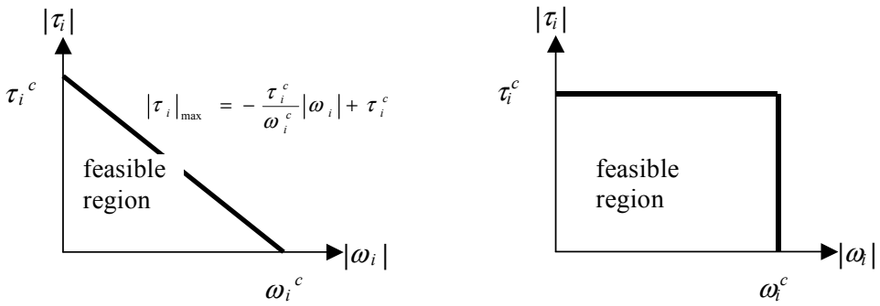

Fig. 1. Two kinds of actuator characteristics; (a) actuator force limit depends on joint velocity, (b) the limits of actuator force and joint velocity are constant.

2.2 Optimization in a Function Space

The equations of motions for a manipulator arm are as follows:

$$\tau = \mathbf{M}(\theta)\alpha + \mathbf{v}(\theta, \omega) + \mathbf{g}(\theta) \tag{6}$$

where $\boldsymbol{\tau}$ denotes the generalized actuator forces ($n \times 1$); $\mathbf{M}$ is the inertia matrix ($n \times n$); $\boldsymbol{\theta}$, $\boldsymbol{\omega}$, and $\boldsymbol{\alpha}$ are the generalized joint displacements, velocities, and accelerations ($n \times 1$), respectively; $\mathbf{v}$ is the centrifugal and coriolis forces ($n \times 1$); and $\mathbf{g}$ is the gravitational force ($n \times 1$).

In this study, four different performance indices are minimized. These are as follows:

$$J_{d1} = \frac{1}{T}\int_0^T \sum_{i=1}^{n} \left(\frac{\tau_i}{\tau_i^c}\right)^2 dt \tag{7}$$

$$J_{d2} = \frac{1}{T}\int_0^T \sum_{i=1}^{n} \left(\frac{\tau_i \omega_i}{\tau_i^c \omega_i^c}\right)^2 dt \tag{8}$$

$$J_{d3} = \frac{1}{T}\int_0^T \sum_{i=1}^{n} \left\{\frac{\tau_i^e}{\tau_i^c} - 1\right\}_+^2 dt \tag{9}$$

$$J_{d4} = \frac{1}{T}\int_0^T \sum_{i=1}^{n} \left[\left\{\frac{\tau_i}{\tau_i^c} - 1\right\}_+^2 + \left\{\frac{\omega_i}{\omega_i^c} - 1\right\}_+^2\right] dt \tag{10}$$

where T is the total motion time and the plus operator $\{\bullet\}_+$ is defined as

$$\{\bullet\}_+ = \begin{cases} \bullet, & if \bullet \geq 0 \\ 0, & if \bullet < 0 \end{cases} \tag{11}$$

(7) and (8) are the performance indices for the minimum torque and minimum energy motions, respectively.

Since τ_i^c and ω_i^c in (7) and (8) simply act as weighting factors of each joint, they do not ensure that the actuator forces and the joint velocities do not exceed their limits. (9) and (10) are the performance indices for the *minimum overload motions*. "Overload'' implies that the actuator forces or the joint velocities exceed their limits. (9) is the case in which the actuator force limits depend on the joint velocities as shown in Fig. 1(a). On the other hand, (10) is the alternate case where the two limits are constant as shown in Fig. 1(b).

If the total motion time is greater than or equal to the minimum time, the minimum values of (9) and (10) must be zero. On the other hand, if it is less than the minimum time, they must be positive. In Section 4, the minimum time motions are defined rigorously by this concept and they are found successfully by the sequential searches for the minimum overload trajectories.

To formulate the obstacle avoidance constraints, we use the so-called *growth function* (Ong & Gilbert, 1996). We briefly review the approach here. Assume that there exists a convex *object* **A** in a three-dimensional workspace. The *object* is defined as a set of all the points inside and on the surface of a rigid body. Let $\mathbf{p}_A$ be an arbitrary point (*seed point*) fixed inside **A**, then the *growth model* $\mathbf{G}_A(\sigma)$ is defined as

$$\mathbf{G}_A(\sigma) = \{\mathbf{y} \mid \mathbf{y} = \mathbf{p}_A + \sigma(\mathbf{x} - \mathbf{p}_A),\ \mathbf{x} \in \mathbf{A}\} \tag{12}$$

where σ is a non-negative scalar.

Consider another convex object **B** in the same workspace and let $\mathbf{G}_B(\sigma)$ be the growth model of **B** wrt. a seed point $\mathbf{p}_B$ fixed inside **B**, then the growth function $\sigma^*(\mathbf{A}, \mathbf{B})$ is defined as follows:

$$\sigma^*(\mathbf{A}, \mathbf{B}) = \min\{\sigma \mid \mathbf{G}_A(\sigma) \cap \mathbf{G}_B(\sigma) \neq \varnothing\} \tag{13}$$

The growth function can be calculated by linear programming if **A** and **B** are convex polyhedra. The dimension of this linear programming problem is 4; thus, the active set method (Best & Ritter, 1985) is efficient for such a low- dimensional LP problem.

Consider that there are m obstacles in a workspace. We assume that all the obstacle models $\mathbf{O}_1,\ldots,\mathbf{O}_m$ and the link models $\mathbf{R}_1(t),\ldots,\mathbf{R}_n(t)$ are convex polyhedra. However, non-convex models are permissible if they can be decomposed into multiple convex models. If the growth function σ^* of a link model $\mathbf{R}_i$ and obstacle model $\mathbf{O}_j$ has a value less than one, one model penetrates into the other and the following *penetration growth distance* D_{ij} indicates the extent of the penetration.

$$D_{ij} = (d_i + d_j)\{1 - \sigma^*(\mathbf{R}_i, \mathbf{O}_j)\}_+ \tag{14}$$

where d_i and d_j are the appropriate positive real numbers that represent the actual geometric sizes of $\mathbf{R}_i$ and $\mathbf{O}_j$, respectively, and the plus operator has been defined above. In general, the penetration growth distance is not equal to the minimum translational distance separating the objects.

From the above notation, the obstacle avoidance constraints become

$$\mathbf{D} = \mathbf{0}, \quad \forall t \in [0, T] \tag{15}$$

where **D** is a matrix ($n \times m$) whose elements are (14).
To obtain obstacle-free optimal motions, we define the following augmented performance indices as

$$J_i = J_{di} + w_o J_o, \quad i = 1, \cdots, 4 \tag{16}$$

where w_o is a sufficiently large weighting coefficient and the obstacle term is

$$J_o = \frac{1}{T} \int_0^T \sum_{i=1}^{n} \sum_{j=1}^{m} (D_{ij})^2 \, dt \tag{17}$$

Motions at the start and goal positions are specified as

$$\theta(0) = \theta_s, \quad \theta(T) = \theta_f \tag{18}$$

$$\omega(0) = \omega_s, \quad \omega(T) = \omega_f \tag{19}$$

$$\alpha(0) = \alpha_s, \quad \alpha(T) = \alpha_f \tag{20}$$

The acceleration conditions (20) are given to assure smooth motions at the start and goal positions.
The obstacle-free optimal motion planning problem can be stated as–

Find $\theta(t)$ ($n \times 1$) that minimize (16) subject to (6), (18) - (20) (21)

The optimal motion planning problem (21) is transformed into a finite-dimensional nonlinear programming problem in the following section.

Nodes(s)	j-3	j-2	j-1	j	j+1	j+2	J+3
$B_j(s)$	0	1/120	26/120	66/120	26/120	1/120	0
$B_j'(s)$	0	1/24	10/24	0	-10/24	-1/24	0
$B_j''(s)$	0	1/6	2/6	-6/6	2/6	1/6	0

Table 1. Nodal values of $B_j(s)$ and its derivatives.

2.3 Optimization in a Finite-Dimensional Vector Space

An infinite number of linearly independent basis functions form a complete set in a function space and this set can represent an arbitrary piece-wise continuous function defined on a closed interval. A finite number of these functions can express a piece-wise continuous function approximately. Many researchers have used cubic *B*-splines as the basis functions. However, in this research, quintic *B*-splines have been used.
Both splines play almost the same role when they are used in robot motion planning. The trajectories expressed by quintic *B*-splines, despite a larger computational burden, have the following merits: 1) Accelerations and jerks are third and second order polynomials, respectively and are therefore continuous; 2) they can express various types of displacement functions more accurately; 3) they have a wider range of feasible directions if used in nonlinear programming; and 4) for a given number of basis functions, the value of the optimal performance indices is usually less than that found using cubic *B*-splines.
The quintic *B*-spline used in this research is (Prenter, 1975)

$$B_j(s) = (1/120)[\{s-(j-3)\}_+^5 - 6\{s-(j-2)\}_+^5 + 15\{s-(j-1)\}_+^5 - 20\{s-j\}_+^5 + 15\{s-(j+1)\}_+^5 - 6\{s-(j+2)\}_+^5 + \{s-(j+3)\}_+^5], \quad s\in[-\infty,\infty] \tag{22}$$

where j is an arbitrary integer. The basis function $B_j(s)$ is positive for $j-3 < s < j+3$ and zero otherwise. The nodal values of (22) and its s-derivatives are listed in Table 1.

If we choose $[0, k]$ as the interval of the parameter s to express the manipulator motions in the time interval $[0, T]$, then $k+5$ splines i.e., $B_{-2}(s),\ldots,B_{k+2}(s)$ have nonzero values in $[0, k]$. The joint trajectories are expressed by the linear combinations of the $k+5$ splines as follows:

$$\theta(s) = \mathbf{C}\,\mathbf{B}(s) \tag{23}$$

$$s = \beta t \tag{24}$$

where s is a dummy variable connecting joint variables with time; $\mathbf{C}$, a coefficient matrix ($n \times k+5$); $\mathbf{B}(s)$, a column vector ($k+5 \times 1$) whose elements are $B_{-2}(s),\ldots,B_{k+2}(s)$; and β ($=k/T$), a time-scale factor that defines the motion time. Thus, k remains constant although the total motion time varies.

Differentiating (23) wrt. time

$$\omega(s) = \beta\,\mathbf{C}\,\mathbf{B}'(s) \tag{25}$$

$$\alpha(s) = \beta^2\,\mathbf{C}\,\mathbf{B}''(s) \tag{26}$$

where the primes (', '') imply differentiation wrt. s.

The initial and final motion conditions (18)–(20) can be used to reduce the dimension of the coefficient matrix. By algebraic manipulation (Park & Bobrow, 2005), the joint trajectories satisfying the initial and final motion conditions are written as follows:

$$\theta(s) = \mathbf{F}_s(s) + \mathbf{C}_m\mathbf{B}_m(s) + \mathbf{F}_f(s) \tag{27}$$

where the boundary condition splines $\mathbf{F}_s(s)$ and $\mathbf{F}_f(s)$, each of dimension ($n \times 1$), can be determined from the initial and final motion conditions. $\mathbf{C}_m$ is *the reduced coefficient matrix* ($n \times k-1$) and $\mathbf{B}_m(s)$ is *the reduced B-spline basis function* ($k-1 \times 1$).

The velocities and accelerations are

$$\omega = \beta\left[\mathbf{F}_s'(s) + \mathbf{C}_m\mathbf{B}_m'(s) + \mathbf{F}_f'(s)\right] \tag{28}$$

$$\alpha = \beta^2\left[\mathbf{F}_s''(s) + \mathbf{C}_m\mathbf{B}_m''(s) + \mathbf{F}_f''(s)\right] \tag{29}$$

(27) together with (24) implies that the arbitrary joint trajectories subject to the initial and final motion conditions are represented approximately by a point in an $n(k-1)$-dimensional linear vector space spanned by the reduced coefficient matrix $\mathbf{C}_m$.

The obstacle-free optimal motion planning problem (21) can be stated as–

$$\textbf{Find } \mathbf{C}_m \in \mathcal{R}^{n(k-1)} \textbf{ that minimizes (16) subject to (6), (27)-(29)} \tag{30}$$

3. Nonlinear Programming using a Quasi-Newton Method

3.1 BFGS Method

If the initial and final motion conditions are given, we can calculate the objective functional (16) by assigning arbitrary specific values to $\mathbf{C}_m$. Along the successive search directions determined by the BFGS algorithm (Fletcher, 1987), we can find the optimal $\mathbf{C}_m^*$.

The first convergence criterion is

$$\left(J_i^{*j-1} - J_i^{*j}\right) \Big/ J_i^{*j-1} \le \varepsilon_1 , \quad i = 1, \cdots, 4 \tag{31}$$

where J_i^{*j} is the minimum value of (16) at the end of the j^{th} line search.
If (31) is satisfied, the following condition is tested to terminate the process:

$$J_o \le \varepsilon_2 \tag{32}$$

The algorithm is:

1. Choose the number k that is at the end of s-interval and choose the total motion time T.
2. Using the motion conditions (18)–(20), calculate the coefficients of the boundary condition splines $\mathbf{F}_s(s)$ and $\mathbf{F}_f(s)$ in (27) (Park & Bobrow, 2005).
3. Determine the initial values of $\mathbf{C}_m$ (Park & Bobrow, 2005).
4. Divide the s-interval [0, k] into l equal subintervals, where, $3k$–$5k$ is appropriate as l.
5. At l +1 nodal points including the two end points, calculate
   5.1. Joint displacements, joint velocities, and joint accelerations (27)–(29), where the s-derivatives are calculated analytically beforehand.
   5.2. Actuator forces (6), which are calculated by outward and inward iteration method (Craig, 1986), and equivalent forces (2).
   5.3. Penetration growth distances (14) between individual link models and individual obstacle models.
6. Calculate one of the four performance indices (7)–(10) and (17) by the trapezoidal integral formula.
7. Determine the initial value of w_o in (16) so that the second term of (16) is about ten times as much as the first term.
8. Calculate the gradient of (16) wrt. $\mathbf{C}_m$ numerically.
9. Determine the search direction by the BFGS method.
10. Perform the line search by the golden section search method.
11. If (31) is satisfied, go to next step; otherwise, go to Step 8.
12. If (32) is satisfied, terminate the process; otherwise, increase w_o by about 10 times and go to Step 8.

The gradient in Step 8 is calculated by the central difference method as follows:

$$(\mathbf{G})_{ij} \cong \frac{J\left((\mathbf{C}_m)_{ij} + \delta\right) - J\left((\mathbf{C}_m)_{ij} - \delta\right)}{2\delta} , \quad i = 1, \cdots, n , \quad j = 1, \cdots, k-1 \tag{33}$$

The B-spline basis functions have certain merits. Since a B-spline has a nonzero value in a small interval, the increment of the objective functional (16) in the small interval is the only data required to calculate the corresponding component of the gradient.
The radii of the minimum circumscribed spheres of the two models are appropriated as the values of the parameters d_i and d_j in (14). k in Step 1 has an effect on the accuracy of the joint trajectories and l in Step 4 has an effect on the accuracy of the numerical integrations. 15 or 20 is assigned to k. 10^{-12}, 10^{-7}, and 10^{-7} are assigned to ε_1, ε_2, and δ, respectively, in the double precision numerical process. All programs have been written in FORTRAN, not using any type of package programs that include IMSL libraries. It takes about ten minutes in the Hewlett Packard workstation x2000 to obtain the optimal motions for a Puma 560 type of manipulator arm in the presence of one hexahedral obstacle.

3.2 Global Search in an Obstacle Field

The numerical optimization described above can be modified to search for the global optimum motions in a given obstacle field. The modification involves repeating the implementations mentioned in Section 3.1 while changing the positions of the seed points of the obstacles. If a link model penetrates into an obstacle model during the optimization process, the path is updated so that the Euclidean distance between the two seed points of the link model and the obstacle model increases. If we locate the seed point in an inner corner of the obstacle model, the link tends to avoid the obstacle by turning around the opposite vertex. By changing the locations of the seed points, we can find all the local minima and choose the global one that has the least minimum performance indices. Although we have no proof that this method will always produce the global minima, it has done so for all of the examples we have solved, including those discussed in this chapter.

4. Minimum Time Motions

If the models of a manipulator and obstacles, and the actuator characteristics are specified, the minimum overloads J_{d3}^*, J_{d4}^* are functions of the total motion time T. Thus, we can define the minimum times as follows:

Definition (Minimum times)

The minimum times $T_i^* \equiv \min \{ T \mid J_{di}^*(T) = 0 \}$, $i = 3, 4$.

Theorem

For an obstacle-free point-to-point manipulator motion, if $T < T_i^*$, then the minimum overloads $J_{di}^*(T) > 0$, $i = 3, 4$. If $T \geq T_i^*$, then $J_{di}^*(T) = 0$, $i = 3, 4$.

Proof

For $T < T_i^*$ and the fact that $J_{di}(T)$ in (9) and (10) are non-negative, the above definition implies that $J_{di}^*(T) > 0$, $i = 3, 4$. For $T \geq T_i^*$ and the fact that $J_{di}^*(T)$ in (9) and (10) are monotonically decreasing functions of T, $J_{di}^*(T_i^*) = 0$ and it must remain zero for all $T \geq T_i^*$, $i = 3, 4$.

The theorem shows that as we increase the motion time T, starting from a time less than T^*, at some point we will achieve T^* if such a time exists. Thus, a simple line search can be used to find T^*. However, we achieved superior performance with the heuristic algorithm (Park & Bobrow, 2005). Detailed explanations are omitted in this chapter. The heuristic algorithm is not the only method but the problem of efficiency to find T^*.

5. Simulations

5.1 Example 1 (Spatial 3-Link Manipulator)

The model is a 3-link arm shown in Fig. 2, where all joints are revolute pairs around their z axes, and it is a configuration at zero-displacement. The base coordinates are the same as the first link coordinates. The specifications are listed in Table 2; in this case, gravity acts in the z_0 direction and τ_c is about twice the static actuator torque necessary to endure gravity in the fully stretched configuration. The sizes of the two hexahedral obstacles are the same and their dimensions are (0.4, 0.4, 0.5) m and the centers are (0.76, –0.47, –0.25) and (0.76, 0.47, 0.25) m in base coordinates. The orientations of the obstacles are equal to the base coordinates. The seed points of all the links are at their geometric centers, but those of all the

obstacles are located in the corners in order to find the various local paths. The manipulator moves from (–60°, 30°, -60°) to (60°, –30°, –120°) in the joint space. The velocities and accelerations at the two end points are zero.

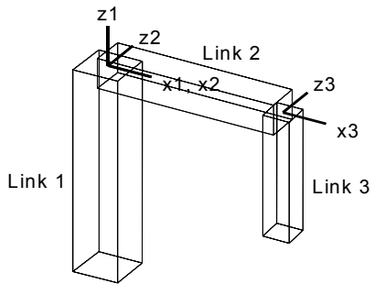

Fig. 2. Spatial 3-link manipulator.

Links	Masses	l_x, l_y, l_z (in link coor.)	τ_c	ω_c
1st	100	0.2, 0.2, 1.0	1000	6
2nd	50	0.8, 0.15, 0.15	1000	6
3rd	30	0.12, 0.6, 0.12	200	6

Table 2. Specifications of Example 1 (SI units).

We repeated the global search for the minimum overload trajectories, mentioned in Section 3.2, starting from T = 0.6 s and increasing it by 0.01 s; where J_3 in (16) is minimized.
Fig. 3 shows the convergence stability, where the minimum overloads decrease monotonically until they vanish at the minimum times. The convergences are therefore quite stable. This figure also demonstrates that we can find the global optimal trajectory by adjusting the seed points of the obstacles. To check the global search clearly, we aligned the obstacles exactly in the path of the initial motion. We have found four local minima shown in Fig. 4 and we can observe that the local minimum (A) is the global one whose minimum overload is the least among the four.

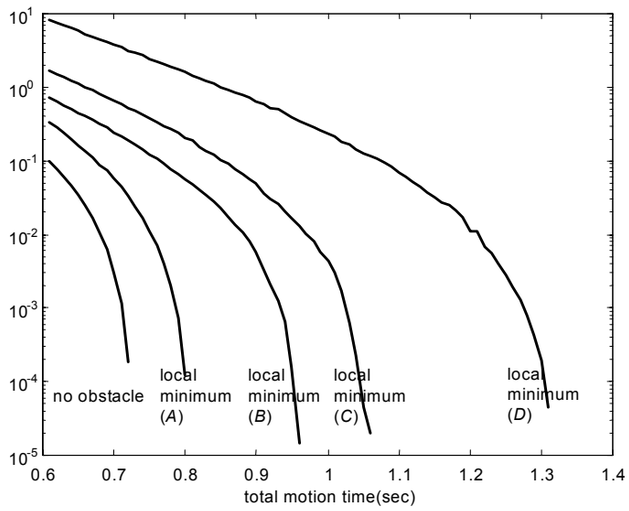

Fig. 3. Minimum overloads J_{d3}^* in Example 1.

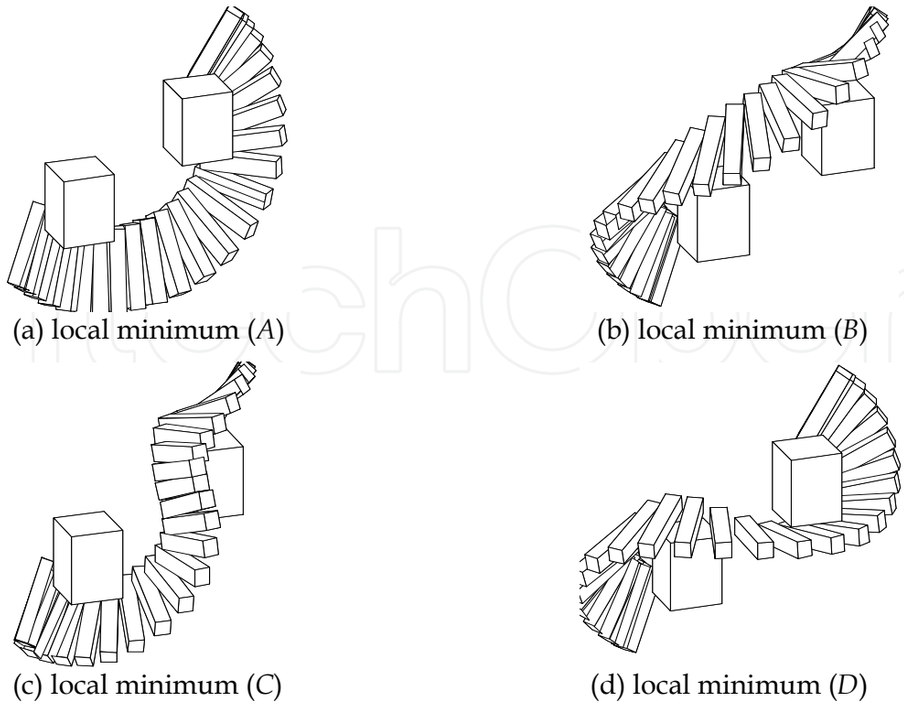

(a) local minimum (*A*) (b) local minimum (*B*)

(c) local minimum (*C*) (d) local minimum (*D*)

Fig. 4. Local minimum trajectories of last link in Example 1

The minimum times are 0.728 s when ignoring the obstacles and 0.807 s, 0.961 s, 1.08 s and 1.32 s in the local minima (*A*)–(*D*), respectively. In the case of no obstacles (not shown in Fig. 4) the manipulator turns around the z_1 axis with Link 3 bent downward to reduce the moment of inertia about that axis and the moment arm of gravity about the z_2 and z_3 axes.
In the optimal motions, the manipulator slightly touches the surfaces of the obstacles; this may be considered as imperfect obstacle avoidance. The minimum clearance to assure safe avoidance must be added to the actual geometric sizes of the obstacles.

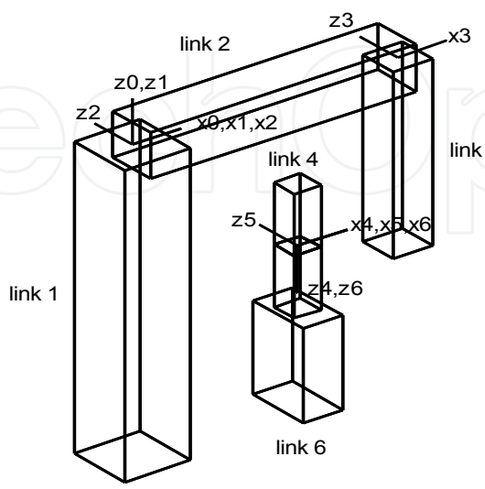

Fig. 5. Spatial 6-link manipulator.

Links	a_{i-1}	a_{i-1}	d_i	θ_i
1st	0	0	0	θ_1
2nd	-90°	0	0	θ_2
3rd	0	0.8	0	θ_3
4th	-90°	0	0.8	θ_4
5th	90°	0	0	θ_5
6th	-90°	0	0	θ_6

Table 3. Link parameters in Denavit-Hartenberg notation of Example 2 (SI units).

5.2 Example 2 (Spatial 6-Link Manipulator)

Fig. 5 shows a configuration of a PUMA 560 type of manipulator at zero-displacement. All joints are revolute pairs around their z axes.

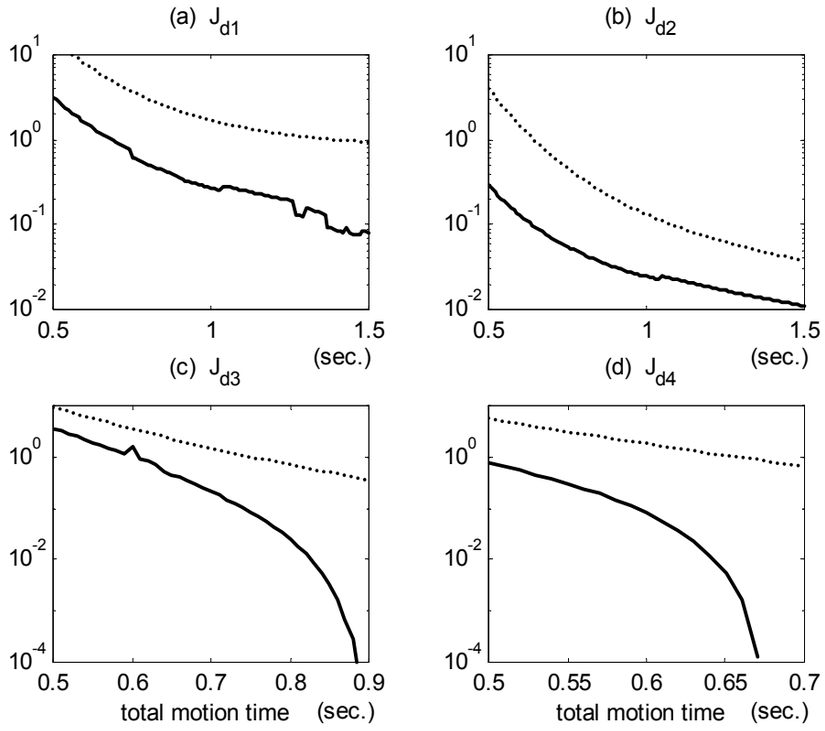

Fig. 6. Initial (upper curves) and minimum (lower curves) performance indices vs. total motion time in Test 1 of Example 2.

The base coordinates are the same as the first link coordinates at zero-displacement. Link 4 is connected to Link 3. The link parameters in the Denavit-Hartenberg notation and the specifications are listed in Table 3 and 4, respectively; in this case, gravity acts in the $-z_0$ direction and τ_c is about twice the static actuator torque necessary to endure gravity in the fully stretched configuration. The mass of the last link includes that of a tool and is heavier than Link 5. The dimensions of one hexahedral obstacle are (1.2, 2.0, 1.2) m and the center is (1.2, 0.0, 0.0) m in base coordinates. The orientation of the obstacle is equal to the base coordinates. The velocities and accelerations at the start and goal positions are all zero.

Links	Mass	l_x, l_y, l_z (in link coor.)	τ_c	ω_c
1st	100	0.2, 0.2, 1.0	1500	6
2nd	50	0.8, 0.15, 0.15	1500	6
3rd	30	0.12, 0.6, 0.12	500	6
4th	5	0.08, 0.08, 0.2	75	6
5th	5	0.08, 0.2, 0.08	75	6
6th	10	0.12, 0.2, 0.3	5	6

Table 4. Specifications of Example 2 (SI units).

Test 1

The manipulator moves from (–20°, 60°, –120°, 0°, –30°, 0°) to (20°, –60°, –60°, 0°, 30°, 0°) in the joint space without considering the obstacle. 20 and 80 are assigned to k and l, respectively. The initial joint trajectories are fifth order polynomials that satisfy (18)–(20) (Park & Bobrow, 2005).

To check the stability of convergences and the reliability of solutions, the author repeated the optimization process while increasing the total motion time. Fig. 6 shows the initial (upper curves) and minimum (lower curves) performance indices vs. the total motion time. It is expected that all the four minimum performance indices must decrease gradually as the total motion time increases. However, as shown in this figure, the minimum torque motions (figure (a)) are unstable, especially when the total motion time is greater.

There are various local minimal motions according to the directions in which the links bend. The joint displacements of the minimum torque motions are greater than those of the other three optimal motions and they increase with the total motion time. Thus, the minimum torque motions may converge to different local minimal motions, thus yielding an unstable convergence. On the other hand, the motions that minimize J_{d4} (figure (d)) show the most stable convergences. Fig. 6(c) and 6(d) show that the minimum overloads decrease gradually until they vanish at the minimum times 0.89 s for J_{d3} and 0.67 s for J_{d4}.

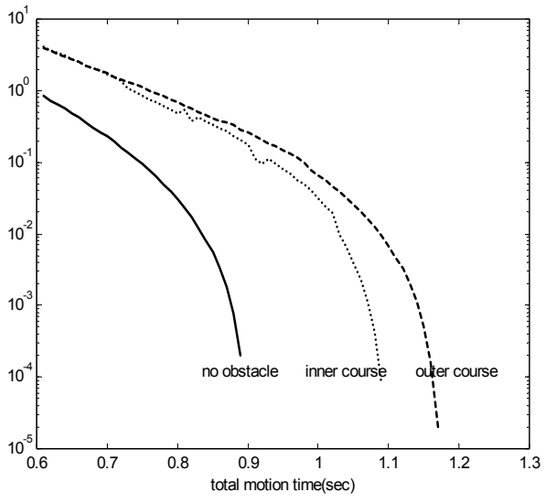

Fig. 7. Minimum overloads J_{d3}^* in Test 2 of Example 2.

Test 2

The manipulator moves from (20°, 60°, –120°, 0°, –30°, 0°) to (–20°, –60°, –60°, 0°, 30°, 0°) in the joint space in the presence of the obstacle described above; where J_3 in (16) is minimized.

Similar to Example 1, we repeated the global search at every time step. The results are shown in Fig. 7. When ignoring the obstacle, the minimum overload decreases gradually until it vanishes at the minimum time 0.90 s. We can see that the convergence is quite stable and it converges to only one optimal motion, regardless of the total motion time. On the other hand, when considering the obstacle, the convergence property in Fig. 7 is not as stable as that in Fig. 3. They converged to different local minima, which will be shown in Fig. 9–12.

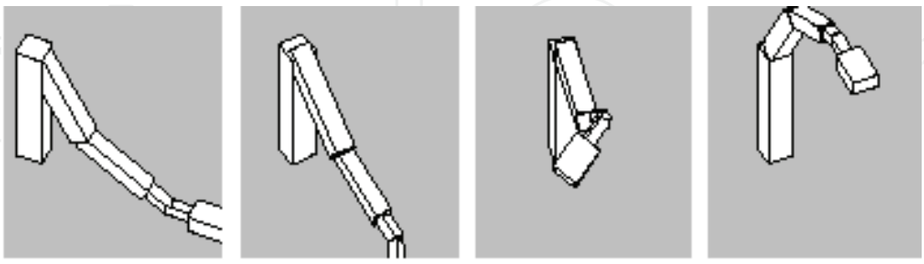

Fig. 8. Minimum time motion ignoring the obstacle.

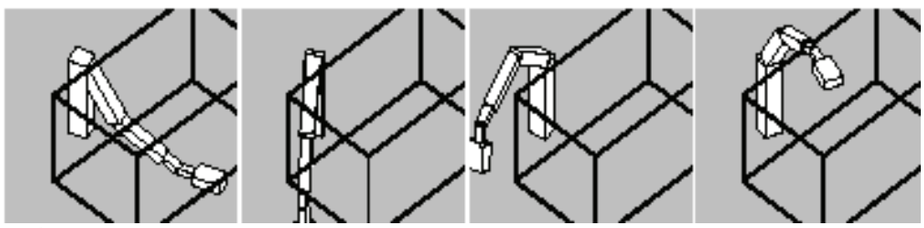

Fig. 9. Local minimum trajectory (*E*) in inner course.

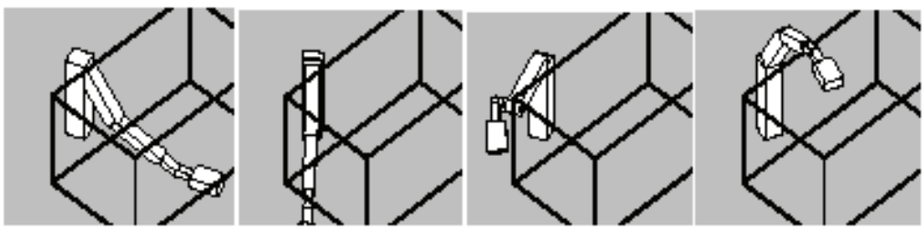

Fig. 10. Local minimum trajectory (*F*) in inner course.

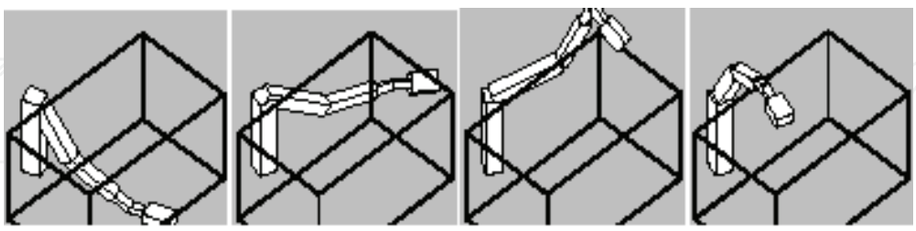

Fig. 11. Local minimum trajectory (*G*) in outer course.

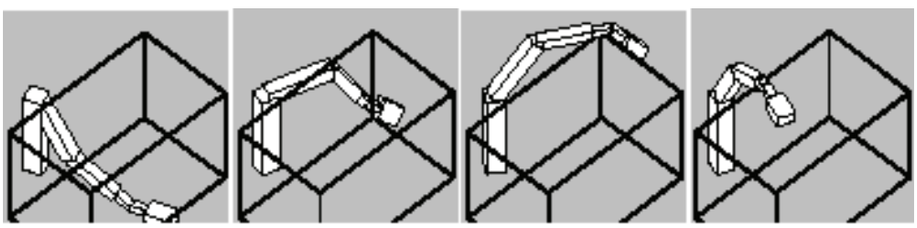

Fig. 12. Local minimum trajectory (*H*) in outer course.

Fig. 8 depicts the minimum time motion, ignoring the obstacle; in this case, the four frames are frames 1, 6, 11, and 16 among the total 16 equal time-interval frames. We can observe in this motion that the manipulator turns around the z_1 axis with the last link bent downward to reduce the moment of inertia about that axis and the moment arm of gravity about the z_2 and z_3 axes. We can also observe that the manipulator maximizes the joint coupling effect by the "overactions" of the "underloaded" joints to reduce the torques of the "overloaded" joints. Here, Joint 1 is "underloaded" and Joints 2 and 3 are "overloaded." We will see these phenomena in Fig. 13 as well. We can see the "overaction" of Joint 1 at the eleventh frame in Fig. 8; that is, Joint 1 turns left over the goal position.

By adjusting the location of the seed point of the obstacle, we have found two obstacle-free courses, namely, the inner and outer courses as shown in Fig. 9–12, where the four frames are frames 1, 6, 11, and 16 among the total 16 equal time-interval frames.

In the inner course, the local minimum shown in Fig. 9 has less minimum overload than Fig. 10. We can observe this fact in Fig. 7, where the curve representing the inner course appears to be composed of several segments of two parallel curves. The difference in the minimum overloads between the two parallel curves becomes smaller as the total motion time approaches the minimum time. Both the minimum times are equal—1.12 s.

In the outer course, the local minimum shown in Fig. 11 has less minimum overload than Fig. 12. The difference is quite small in Fig. 7, but it becomes larger as the total motion time approaches the minimum time. The minimum times in Fig. 11 and 12 are 1.17 and 1.21 s, respectively.

Fig. 13 shows the saturation state of the actuators. Joints 2, 3, and 5 are overloaded in the initial motions (dotted lines), where the maximum equivalent torques exceed twice their actuator limits. After the optimization, the motion time is increased from 0.8 s to 0.90 s in the case of no obstacle and is increased to 1.12 s to avoid the obstacle. Moreover, all the joints are close to saturation during the minimum time motions (solid lines). This is consistent with Pontryagin's maximum principle since a necessary condition for the minimum time motion (assuming no singular arcs) is that all the joints should be in saturation during the motions.

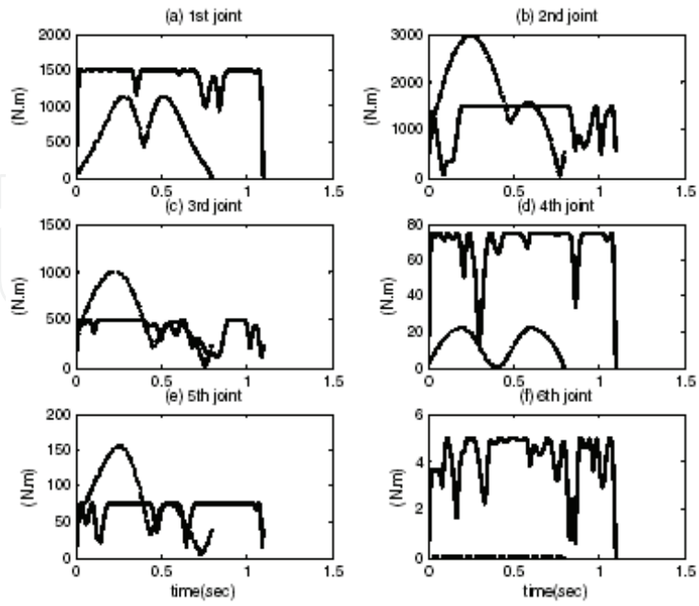

Fig. 13. Equivalent torques in Test 2 of Example 2; solid lines are minimum time motions in local minimum (E) and dotted lines are initial motions, T = 0.8 s.

Our algorithm is not tailored to obstacles moving in dynamic environments. However, if the motions of the obstacles are given as functions of time, we can solve the minimum time problem in exactly the same manner as in this chapter. In the case where obstacles are moving in a dynamic and unpredictable manner in the environment, there is really no method to optimally plan motions around them. Khatib's "elastic bands" could potentially handle this situation, but the solution would be suboptimal.

In future works, we will consider the frictional effects in this method. Our method cannot directly handle Coulomb friction because it creates a discontinuity in the gradients. If the frictional effects are considered successfully, a more effective control method could be found to track this optimal trajectory.

6. Conclusions

In this chapter, we present a practical and reliable method for finding the minimum torque, minimum energy, minimum overload, and minimum time motions for the manipulators moving in an obstacle field, subject to the limits of velocity-dependent actuator forces. Arbitrary point-to-point manipulator motions are represented by a point in a finite-dimensional vector space parameterized by quintic *B*-splines.

The novel idea in this work is the concept of the minimum overload trajectory, in which the actuator-overloads achieve their minimum values with the total motion time fixed. The minimum time motion is defined rigorously with this concept and it is obtained by successive searches for the minimum overload trajectory.

There are various local minimal motions according to the directions in which the manipulator links bend. We can perform global searches in a certain obstacle field by adjusting the locations of the *seed points* of the obstacle models or the link models.

In the resultant optimal motions, the manipulator turns with the last link bent inward in order to reduce the moment of inertia about the z_1 axis and the moment arms of gravity about the z_2 and z_3 axes.

In the resultant minimum time motions, 1) the manipulator maximizes the joint coupling effect by the overactions of underloaded joints to reduce the torques on the overloaded joints, and 2) almost all the actuators are close to saturation during the motion, which is consistent with Pontryagin's maximum principle.

7. References

Bessonnet, G. & Lallemand, J. P. (1994). On the optimization of robotic manipulator trajectories with bounded joint actuators or joint kinetic loads considered as control variables, *Trans. ASME J. Dynamic Systems Measurement and Control*, Vol. 116, 819-826, ISSN 0022-0434

Best, M. J. & Ritter, K. (1985). *Linear Programming: Active Set Analysis and Computer Programs*, Prentice-Hall

Bobrow, J. E.; Dubowsky, S. & Gibson, J. S. (1985). Time-optimal control of robotic manipulators along specified paths, *International J. Robotics Research*, Vol. 4, 3-17, ISSN 0278-3649

Bobrow, J. E. (1988). Optimal robot path planning using the minimum-time criterion, *IEEE J. Robotics and Automation*, Vol. 4, 443-450, ISSN 0882-4967

Bobrow, J. E.; Martin, B.; Sohl, G.; Wang, E. C.; Park, F. C. & Kim, J. (2001). Optimal robot motions for physical criteria, *J. Robotic Systems*, Vol. 18, 785-795, ISSN 0741-2223

Bryson, Jr. A. E. & Meier, E. B. (1990). Efficient algorithm for time-optimal control of a two-link manipulator, *J. Guidance, Control, and Dynamics*, Vol. 13, 859-866, ISSN 0731-5090

Cao, B.; Dodds, G. I. & Irwin, G.. W. (1998). A practical approach to near time-optimal inspection-task-sequence planning for two cooperative industrial robot arms, *International J. Robotics Research*, Vol. 17, 858-867, ISSN 0278-3649

Constantinescu, D. & Croft, E. A. (2000). Smooth and time-optimal trajectory planning for industrial manipulators along specified paths, *J. Robotic Systems*, Vol. 17, 233-249, ISSN 0741-2223

Craig, J. J. (1986). *Introduction to Robotics; Mechanics and Control*, Addison-Wesley, ISBN0201095289

Fenton, R. G.; Benhabib, B. & Goldenberg, A. A. (1986). Optimal point-to-point motion control of robots with redundant degrees of freedom, *Trans ASME J. Engineering for Industry*, Vol. 108, 120-126, ISSN 0022-0817

Fletcher, R. (1987). *Practical Method of Optimization*, 2nd ed., John Wiley & Sons, ISBN0471494631

Formalsky, A. M. (1996). The time-optimal control of the bending of a plane two-link mechanism, *J. Applied Mathematics and Mechanics*, Vol. 60, 243-251, ISSN 0021-8928

Galicki, M. (1998). The planning of robotic optimal motions in the presence of obstacles, *International J. Robotics Research*, Vol. 17, 248-259, ISSN 0278-3649

Galicki, M. & Ucinski, D. (2000). Time-optimal motions of robotic manipulators, *Robotica*, vol. 18, 659-667, ISSN 0263-5747

Hol, C. W. J.; Willigenburg, L. G.; Henten, E. J. & Straten, G. (2001). A new optimization algorithm for singular and non-singular digital time-optimal control of robots, *Proceedings of IEEE International Conference on Robotics and Automation*, 1136-1141, ISBN078036578X

Jouaneh, M. K.; Dornfeld, D. A. & Tomizuka, M. (1990). Trajectory planning for coordinated motion of a robot and a positioning table: part 2, *IEEE Trans. Robotics and Automation*, Vol. 6, 746-759, ISSN 1042-296X

Lee, J. (1995). Dynamic programming approach to near minimum-time trajectory planning for two robots, *IEEE trans. Robotics and Automation*, Vol. 11, 160-164, ISSN 1042-296X

Ong, C. J. & Gilbert, E. G. (1996). Growth distances: new measures for object separation and penetration, *IEEE trans. Robotics and Automation*, Vol. 12, 888-903, ISSN 1042-296X

Ozaki, H. & Lin, C.-j. (1996). Optimal B-spline joint trajectory generation for collision-free movements of a manipulator under dynamic constraints, *Proceedings of IEEE International Conference on Robotics and Automation*, 3592-3597, ISBN0780329880

Park, J.-k. & Bobrow, J. E. (2005). Reliable computation of minimum-time motions for manipulators moving in obstacle fields using a successive search for minimum overload trajectories, *J. Robotic Systems*, Vol. 22, 1-14, ISSN 0741-2223

Prenter, P. M. (1975). *Splines and Variational Methods*, John Wiley & Sons, ISBN0471504025

Schlemmer, M. & Gruebel, G. (1998). Real-time collision-free trajectory optimization of robot manipulators via semi-infinite parameter optimization, *International J. Robotics Research*, Vol. 17, 1013-1021, ISSN 0278-3649

Shiller, Z. & Dubowsky, S. (1991). On computing the global time-optimal motions of robotic manipulators in the presence of obstacles, *IEEE Trans. Robotics and Automation*, Vol. 7, 785-797, ISSN 1042-296X

Shiller, Z. (1994). On singular time-optimal control along specified paths, *IEEE Trans. Robotics and Automation*, Vol. 10, 561-566, ISSN 1042-296X

Shin, K. G. & McKay, N. D. (1985). Minimum-time control of robotic manipulators with geometric path constraints, *IEEE trans. Automatic Control*, AC-30, 531-541, ISSN 0018-9286

Shin, K. G. & Zheng, Q. (1992). Minimum-time collision-free trajectory planning for dual-robot systems, *IEEE trans. Robotics and Automation*, Vol. 8, 641-644, ISSN 1042-296X

Singh, S. K. & Leu, M. C. (1991). Manipulator motion planning in the presence of obstacles and dynamic constraints, *International J. Robotics Research*, Vol. 10, 171-186, ISSN 0278-3649

Wang, C.-Y. E.; Timoszyk, W. K. & Bobrow, J. E. (2001). Payload maximization for open chained manipulators: finding weightlifting motions for a Puma 762 robot, *IEEE trans. Robotics and Automation*, Vol. 17, 218-224, ISSN 1042-296X

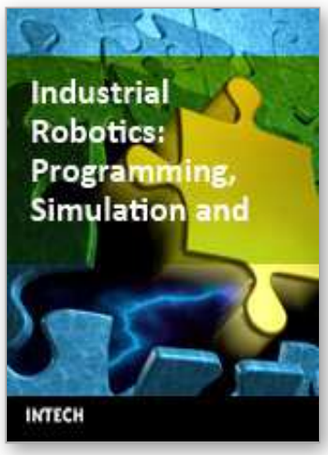

Industrial Robotics: Programming, Simulation and Applications

Edited by Low Kin Huat

ISBN 3-86611-286-6

Hard cover, 702 pages

Publisher Pro Literatur Verlag, Germany / ARS, Austria

Published online 01, December, 2006

Published in print edition December, 2006

This book covers a wide range of topics relating to advanced industrial robotics, sensors and automation technologies. Although being highly technical and complex in nature, the papers presented in this book represent some of the latest cutting edge technologies and advancements in industrial robotics technology. This book covers topics such as networking, properties of manipulators, forward and inverse robot arm kinematics, motion path-planning, machine vision and many other practical topics too numerous to list here. The authors and editor of this book wish to inspire people, especially young ones, to get involved with robotic and mechatronic engineering technology and to develop new and exciting practical applications, perhaps using the ideas and concepts presented herein.

InTech Europe
University Campus STeP Ri
Slavka Krautzeka 83/A
51000 Rijeka, Croatia
Phone: +385 (51) 770 447
Fax: +385 (51) 686 166
www.intechopen.com

InTech China
Unit 405, Office Block, Hotel Equatorial Shanghai
No.65, Yan An Road (West), Shanghai, 200040, China
中国上海市延安西路65号上海国际贵都大饭店办公楼405单元
Phone: +86-21-62489820
Fax: +86-21-62489821

IntechOpen